Supporting Information for

Enhancing Electronic Metal–Support Interaction in Cu-ZnO/N-Carbon Catalysts by Generating More Pyridinic Nitrogen Species for Efficient Hydrogenation of CO_2 to Methanol

Zhiyue Wang [a, b, 1], Yonghui Cheng [a, b, 1], Haipeng Jiang [a], Yibing Song[c] and Zhen Li[c], Moris S. Eisen*[b], Ziyi Zhong*[a, b]

[a] *Department of Chemical Engineering, and Guangdong Provincial Key Laboratory of Materials and Technologies for Energy Conversion (MATEC), Guangdong Technion Israel Institute of Technology (GTIIT), Shantou, 515063, China*

[b] *Schulich Faculty of Chemistry, and Resnick Sustainability Center for Catalysis, Technion-Israel Institute of Technology (IIT), Haifa 32000, Israel*

[c] *College of Chemistry & Chemical Engineering and Key Laboratory for Preparation and Application of Ordered Structural Materials of Guangdong Province, Shantou University, Shantou 515063, China*

*Corresponding authors.

Email address: Ziyi.zhong@gtiit.edu.cn, Moris.eisen@gtiit.edu.cn

[1] These authors contributed equally to this work.

Chemicals

The synthesis of carbon support with various doped-N content required the following chemicals: 3-(3-Aminomethyl) phenol, Resorcinol, Hexamethylenetetramine (HMTA), Pluronic® F127 ((EO)106(PO)70(EO)106), Ammonia solution (25%), DI water, and urea. Among them, 3-(3-Aminomethyl) phenol, Resorcinol, Hexamethylenetetramine (HMTA), and Pluronic® F127 were purchased from Sigma-Aldrich®; Ammonia solution (25%) was purchased from Merck®. The metal precursor - copper nitrate ($Cu(NO_3)_2 \cdot 3H_2O$) and zinc nitrate ($Zn(NO_3)_2 \cdot 6H_2O$) were obtained from Macklin®. All chemicals were of analytical grade (> 99.9% purity) and used as received without further purification. Deionized water (18.25 MΩ·cm) was used throughout the experiments.

Evaluation of internal diffusion limitations using the Weiz-Prater criteria

To determine whether the measured reaction kinetic data represents the intrinsic reactivity of 15% Cu-ZnO/NOMC (0.2)-550 rather than restricted by internal mass transfer due to internal-diffusion limitation, the Weiz-Prater criteria were adopted to estimate the Thiele modulus (Φ) and effectiveness (η) under the reaction condition (250 C, 30 bar), and it is calculated using the following expression [1]:

$$C_{wp} = \frac{r_{obs} \cdot L_p^2}{D_{eff} \cdot C_{as}} = \eta\, \Phi^2$$

Based on the high BET surface area (around 550 m^2/g_{cat}), the effective diffusivity (D_{eff}) was conservatively estimated at 1×10^{-7} m^2/s, which is based on a random pore model [2] and high-pressure gas diffusion in porous media [3] by assuming a tortuosity factor of $\tau \approx 3$ [4]. For catalyst powder sieved to 100-120 mesh with an averaged particle size d_p=135 μm, the characteristic length is determined to be 2.25×10^{-5} m ($L_p=d_p/6$). The observed volumetric reaction rate (r_{obs}) is derived from the obtained STY_{CH3OH} of 9.2 $mmol_{CH3OH}\ g_{cat}^{-1}\ h^{-1}$ and the particle's density (ρ_p=0.8g/cm^3), yielding a value of 2.1 $mol_{CH3OH}/m^3_{cat}\cdot s$. The bulk gas concentration is derived from the following ideal gas formula:

$$C_{as} = \frac{n_{CO2}}{v} = \frac{P \cdot y_{CO2}}{RT} = 172\ mol/m^3$$

Where P is the overall operational pressure, y represents the CO_2 molar fraction, R represents the ideal gas constant (8.314 $\frac{l}{kpa \cdot mol \cdot l}$), and T is the reaction temperature in kelvin (523.15 K). The resulted Cwp value is determined to be 6.1×10^{-5} which is several orders of magnitude below the threshold value (C_{wp}=0.1)

The resulted effectiveness (η) approached unity and the Thiele modulus (Φ) is approximated to be 7.8×10^{-3}, suggesting a much higher internal diffusion rate than the reaction rate. Therefore, we can say that the system is reaction rate-limiting and the internal mass transfer limitation is negligible.

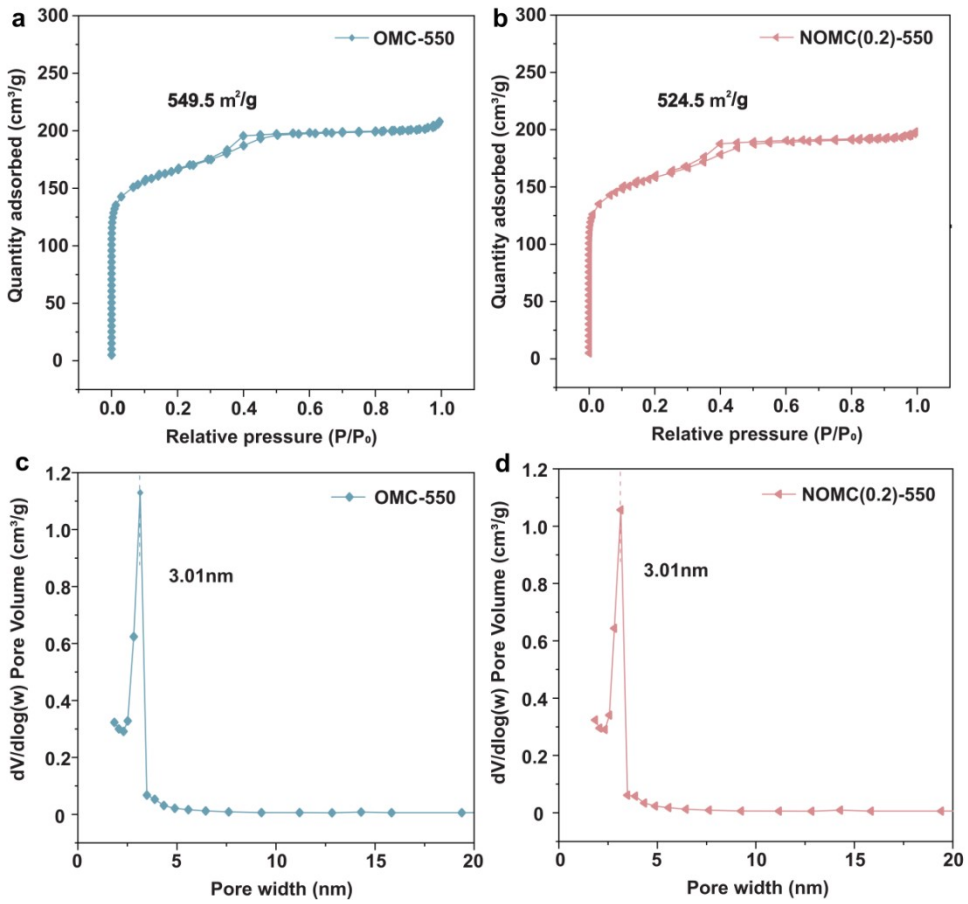

Fig. S1. (a, b) Nitrogen adsorption/desorption isotherms and (c, d) pore size distributions of the OMC-550 and NOMC(0.2)-550 supports.

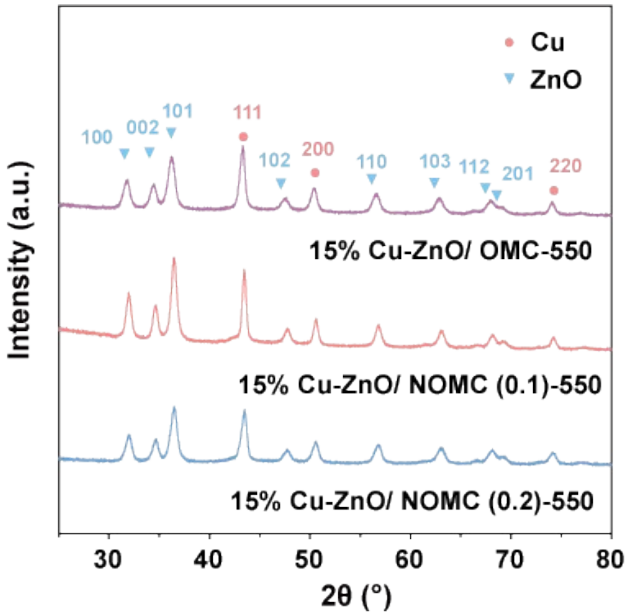

Fig. S2. XRD patterns of the Cu–ZnO catalysts supported on NOMC(0.2) with different metal loadings ratios.

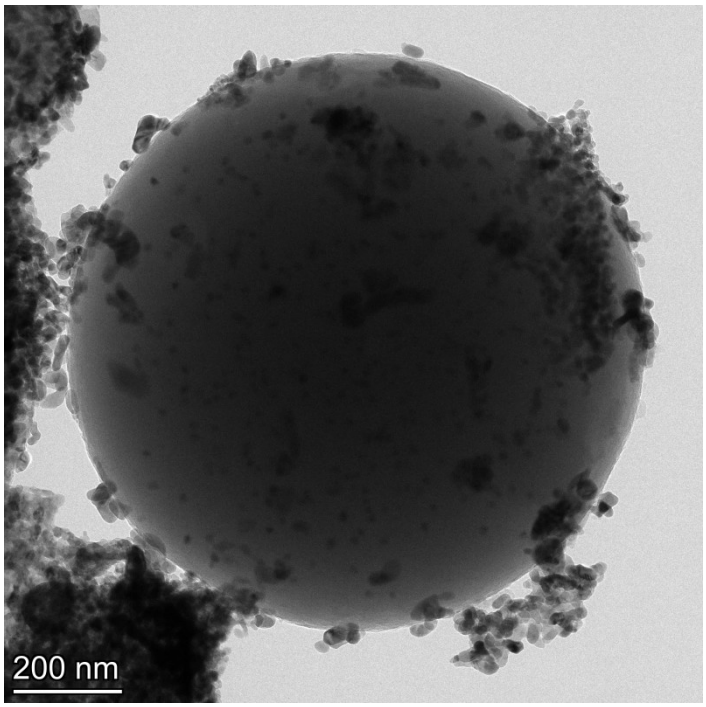

Fig. S3. TEM images of the 15 wt% Cu–ZnO/OMC-550 catalyst.

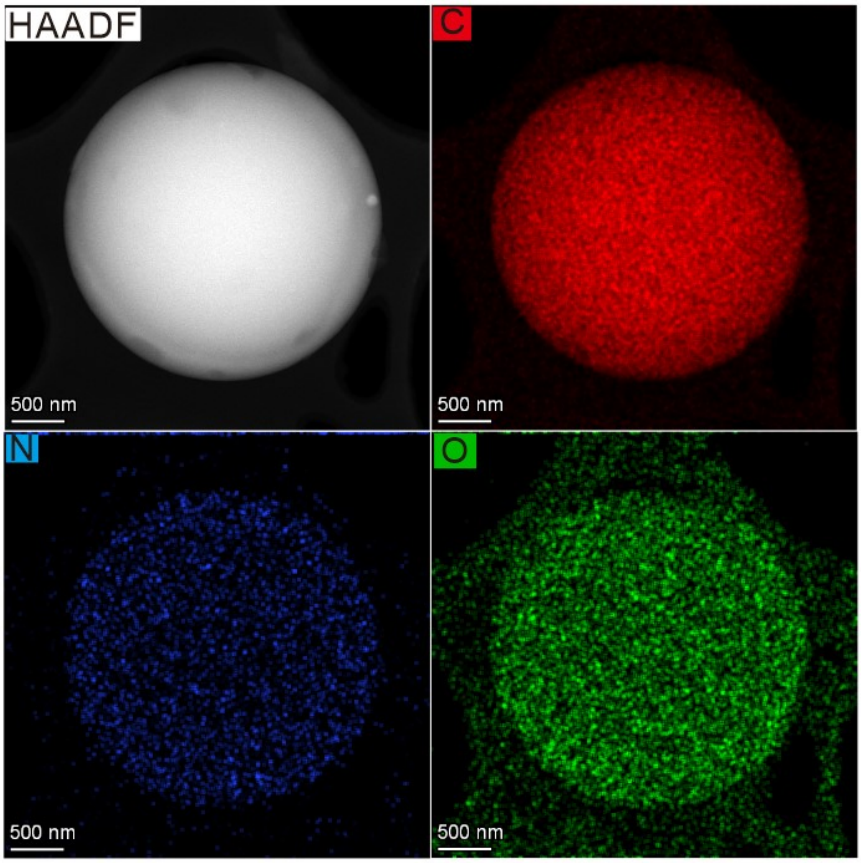

Fig. S4. HAADF-STEM image of the pure NOMC(0.2) support with the corresponding EDS elemental mapping analysis.

.

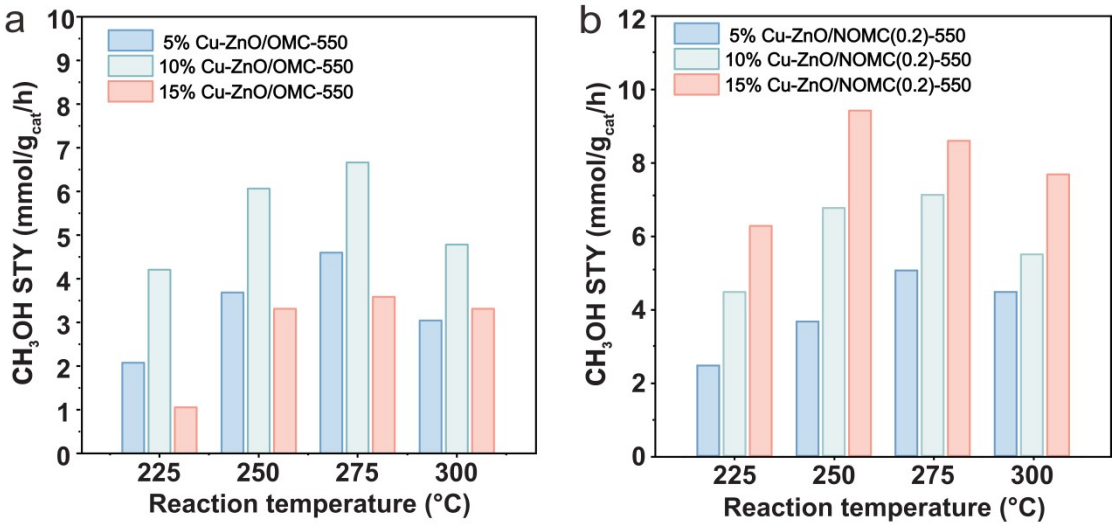

Fig. S5. The measured methanol STY values with increasing amount of Cu-ZnO loading on 550 ℃ calcined (a) carbon support without N doping, (b) NOMC(0.2) carbon support (Reaction conditions for catalytic test: Gas flow rate =15 ml/min, $H_2/CO_2/Ar=72/24/4$, $P_{tot}=3.0MPa$).

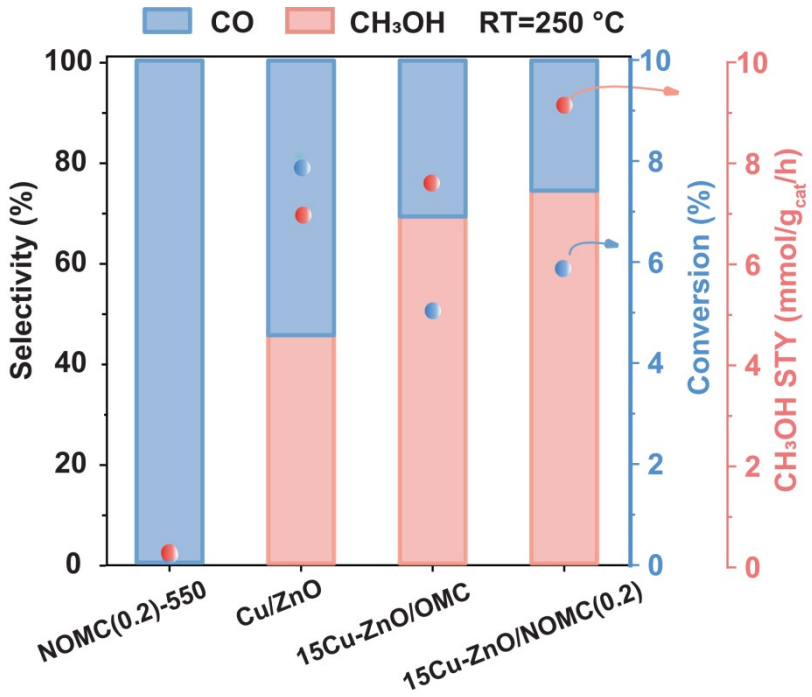

Fig. S6. Control experiments to verify the synergistic effect between Cu-ZnO active sites and the NOMC support. (Reaction conditions: 250 °C, 3.0 MPa, H_2/CO_2 = 3:1).

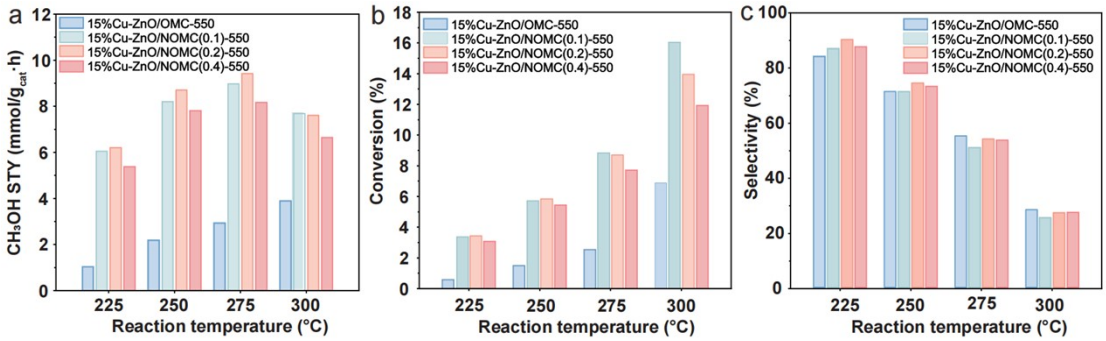

Fig. S7. The measured (a) methanol STY, (b) CO_2 conversion, and (c) product selectivity toward methanol over a series of Cu-ZnO/NOMC catalysts with increasing doped-N content and 15 wt% Cu–ZnO calcined at 550ºC in a reaction temperature range from 225 ºC to 300 ºC (Reaction conditions for catalytic test: Gas flow rate =15 ml/min, $PH_2/PCO_2/PAr=72/24/4$, $P_{tot}=3.0$ MPa).

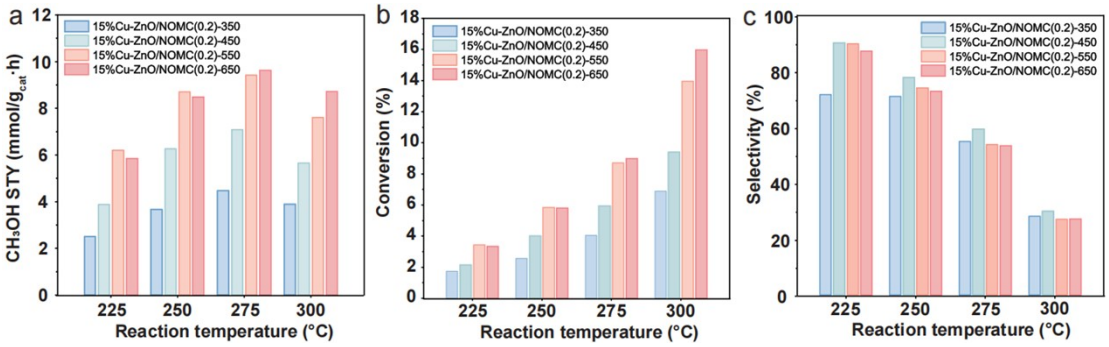

Fig. S8. The measured (a) methanol STY; (b) CO_2 conversion; (c) selectivity toward methanol as the function of increasing support's carbonization temperature from 350 ℃ to 650 ℃ under the 15 wt% Cu–ZnO (Reaction conditions for catalytic test: Gas flow rate =15 ml/min, $PH_2/PCO_2/PAr=72/24/4$, $P_{tot}=3.0$ MPa).

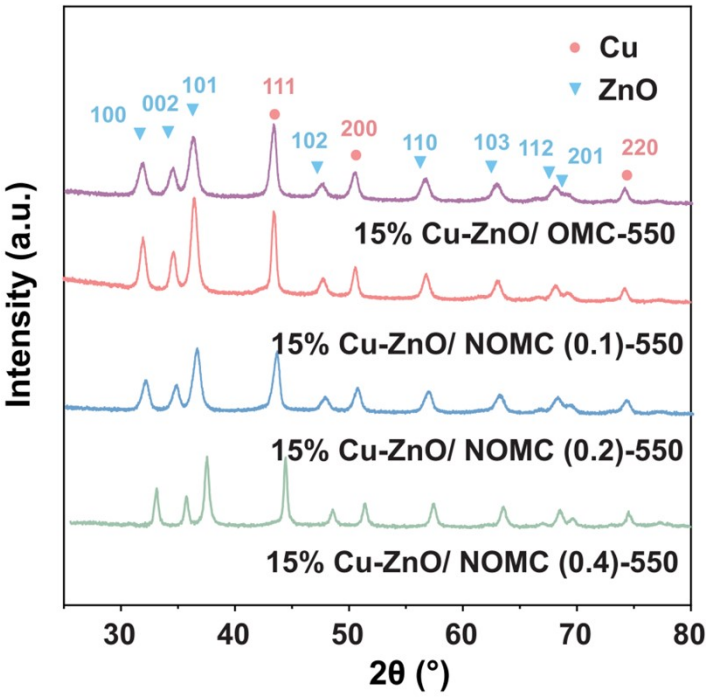

Fig. S9. XRD patterns of the spent 15% Cu–ZnO catalysts supported on different ratio of nitrogen doped carbon supports.

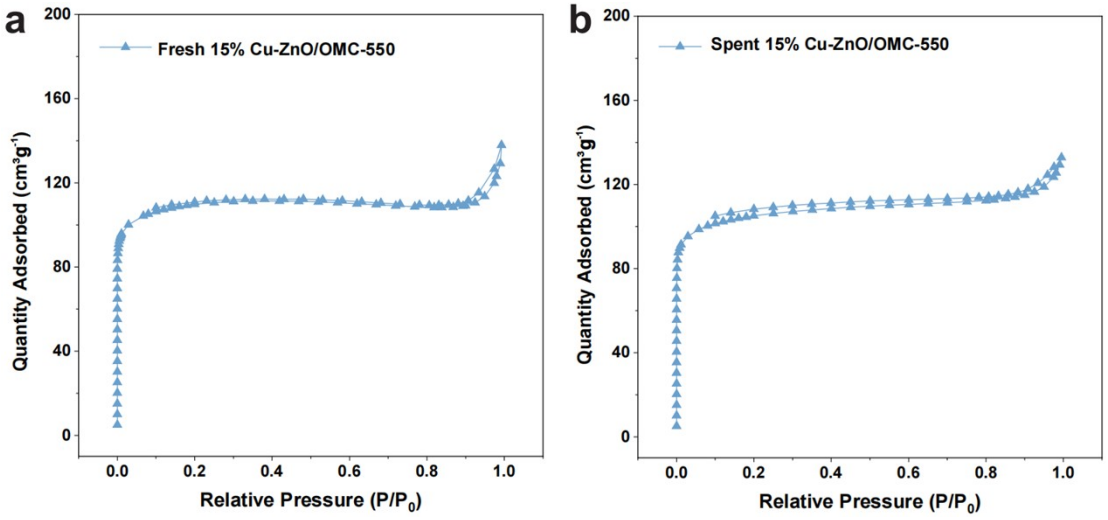

Fig. S10. (a, b) Nitrogen adsorption/desorption isotherms of the Fresh 15% Cu-ZnO/OMC-550 and Spent 15% Cu-ZnO/OMC-550 catalyst.

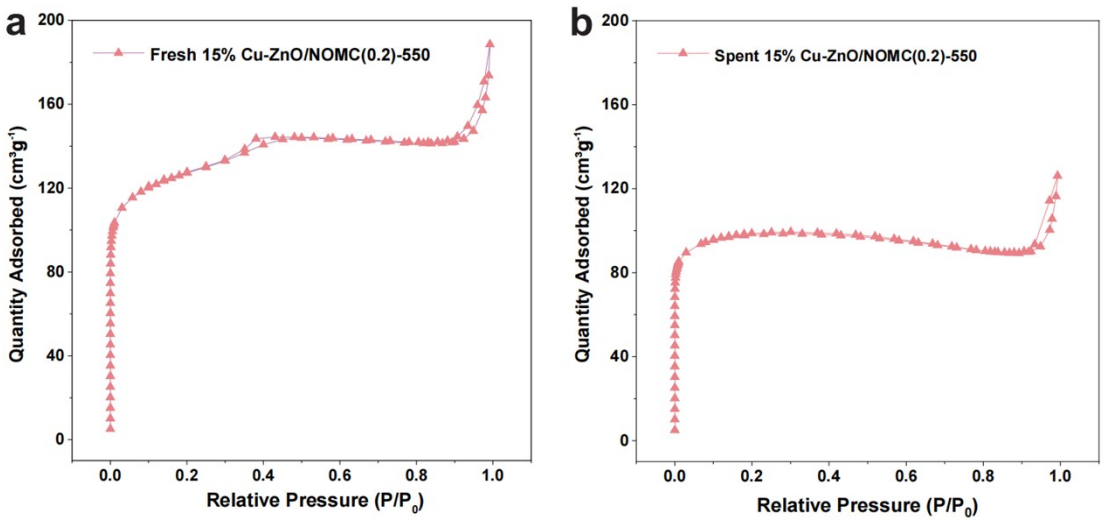

Fig. S11. (a, b) Nitrogen adsorption/desorption isotherms of the Fresh 15% Cu-ZnO/NOMC (0.2)-550 and Spent 15% Cu-ZnO/NOMC (0.2)-550 catalyst.

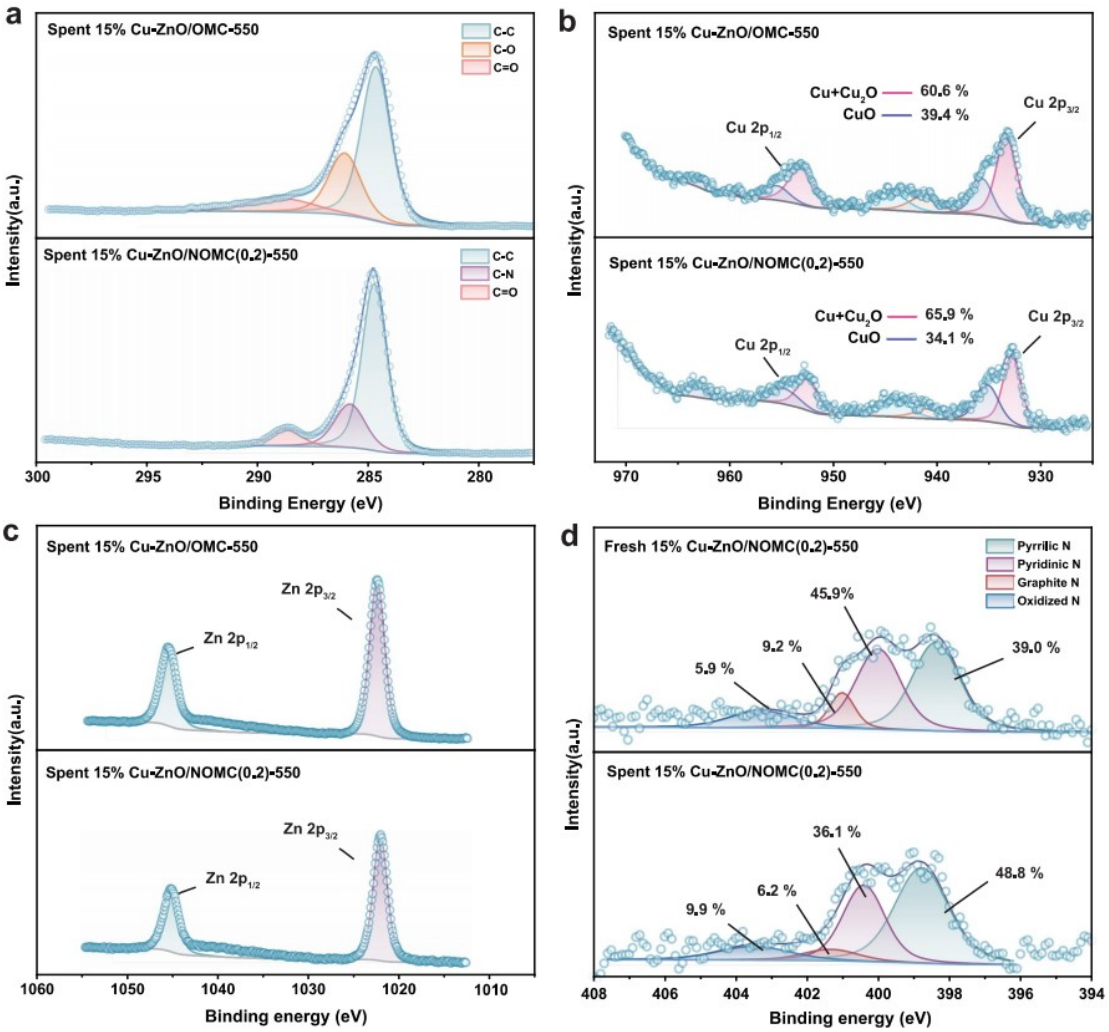

Fig. S12. High-resolution XPS spectra of the fresh and the spent catalysts. (a) C 1s spectra of the spent 15% Cu-ZnO/OMC-550 and 15% Cu-ZnO/NOMC(0.2)-550 catalysts. (b) Cu 2p spectra of the spent 15% Cu-ZnO/OMC-550 and 15% Cu-ZnO/NOMC(0.2)-550 catalysts, with the relative contents of Cu^0/Cu^+ and Cu^{2+} species labeled. (c) Zn 2p spectra of the spent 15% Cu-ZnO/OMC-550 and 15% Cu-ZnO/NOMC(0.2)-550 catalysts. (d) N 1s spectra of the fresh and the spent 15% Cu-ZnO/NOMC(0.2)-550 catalysts, with the relative contents of pyrrolic N, pyridinic N, graphitic N and oxidized N species labeled. All binding energies were calibrated using the adventitious C 1s peak at 284.8 eV.

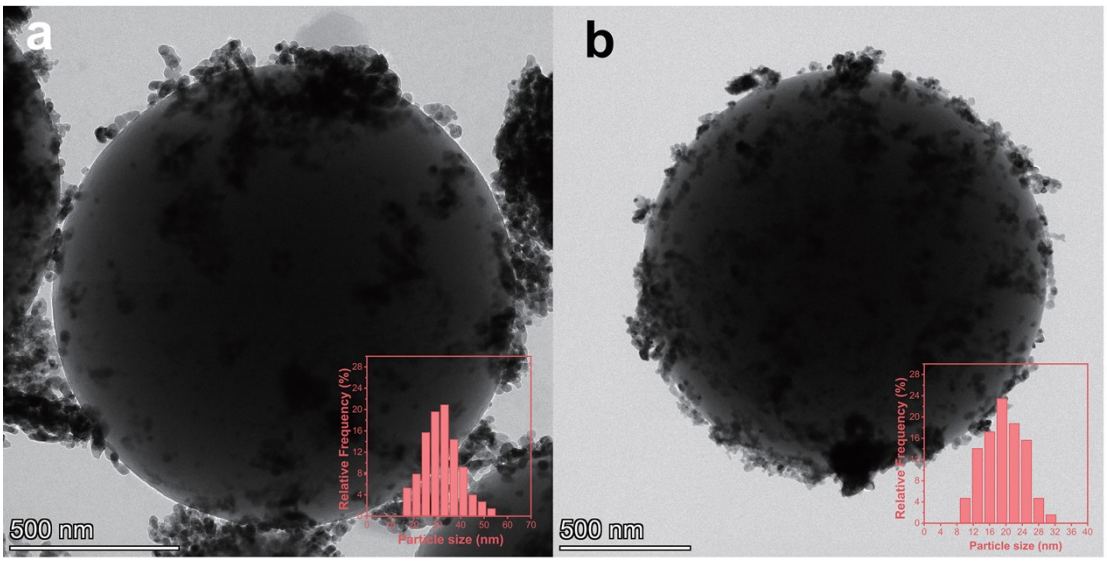

Fig. S13. TEM images of the spent catalysts after a 70h of CO_2 hydrogenation reaction. (a) The spent 15% Cu-ZnO/OMC-550 catalyst; (b) the spent 15% Cu-ZnO/NOMC(0.2)-550 catalyst. The insets show the corresponding particle size distribution histograms of Cu-ZnO nanoparticles, obtained by counting over 200 randomly selected particles.

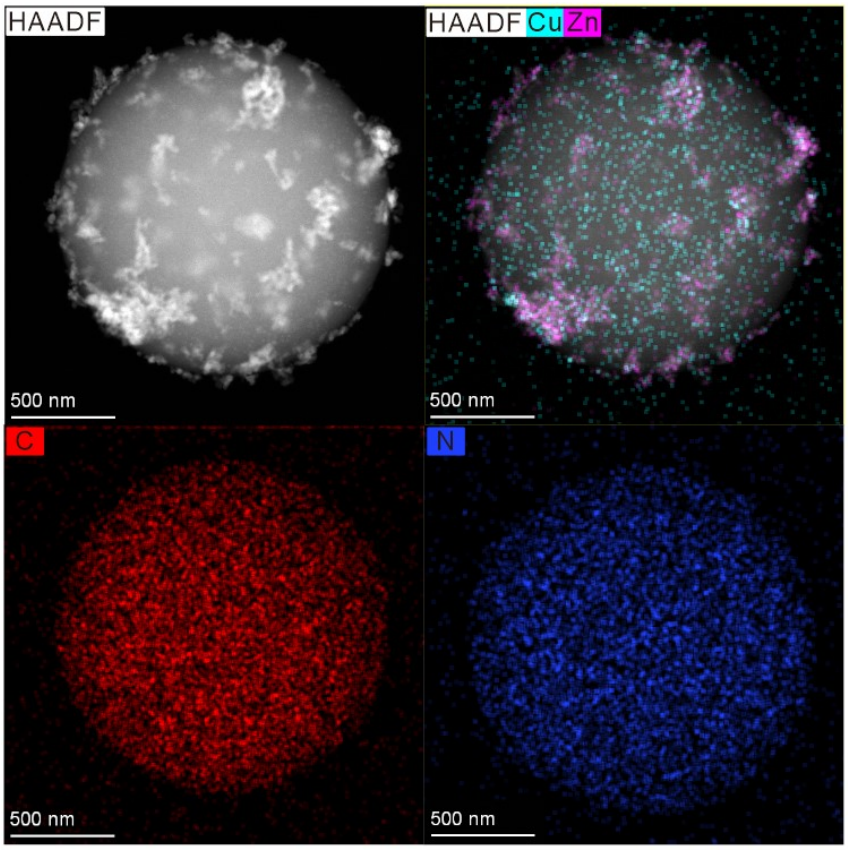

Fig. S14. HAADF-STEM image and corresponding EDX elemental mapping of the spent 15% Cu-ZnO/NOMC(0.2)-550 catalyst. (Top left) HAADF-STEM image; (Top right) Overlaid elemental mapping of Cu (cyan) and Zn (purple); (Bottom left) Elemental mapping of C (red); (Bottom right) Elemental mapping of N (blue).

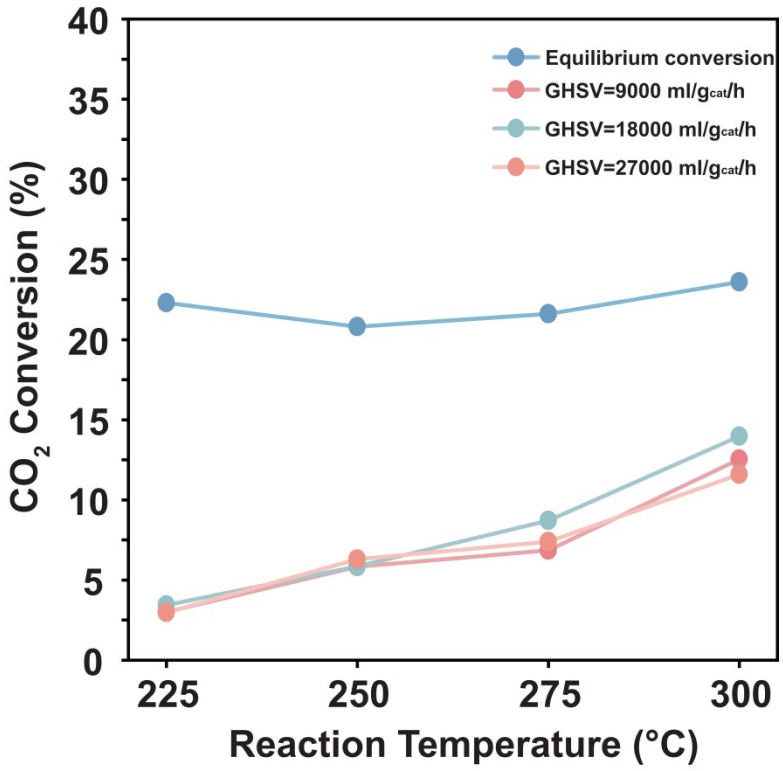

Fig. S15. Comparison of experimental CO_2 conversion with thermodynamic equilibrium conversion as a function of reaction temperature. Data are shown for different gas hourly space velocities (GHSV = 9000, 18000, and 27000 mL g cat^{-1} h^{-1}) under standard reaction conditions (3.0 MPa, H_2/CO_2 = 3:1). The equilibrium conversion was calculated using thermodynamic data, confirming that all experimental measurements are well below the thermodynamic limit.

The CO_2 equilibrium conversion [5] was compared to the experimental CO_2 conversion, as shown in Figure S15. The results indicated that the experimental CO_2 conversions were consistently below the equilibrium limit at all reaction temperatures. This demonstrates that CO_2 hydrogenation is primarily governed by kinetic factors rather than thermodynamic ones.

To determine whether the CO_2 conversion reflects the characterized reaction rate or is constrained by the external diffusion limit, we performed parallel experiments by varying the reactant GHSV from 9000 to 27000 ml $gcat^{-1}$ h^{-1} through increasing the reactant flow rate. The original catalyst loading, reactant molar ratio, and other

operational conditions all remained unchanged, ensuring that the increase in GHSV directly corresponds to an enhancement in the linear velocity (u) of the reactant gas.

The results show that STY_{CH3OH} increases linearly with increasing gas flow rate, while CO_2 conversion shows minor fluctuations around 5.8-6.0%. This confirms that the reactant is primarily under kinetic control and that external diffusion was not a rate-determining step under the investigated conditions.

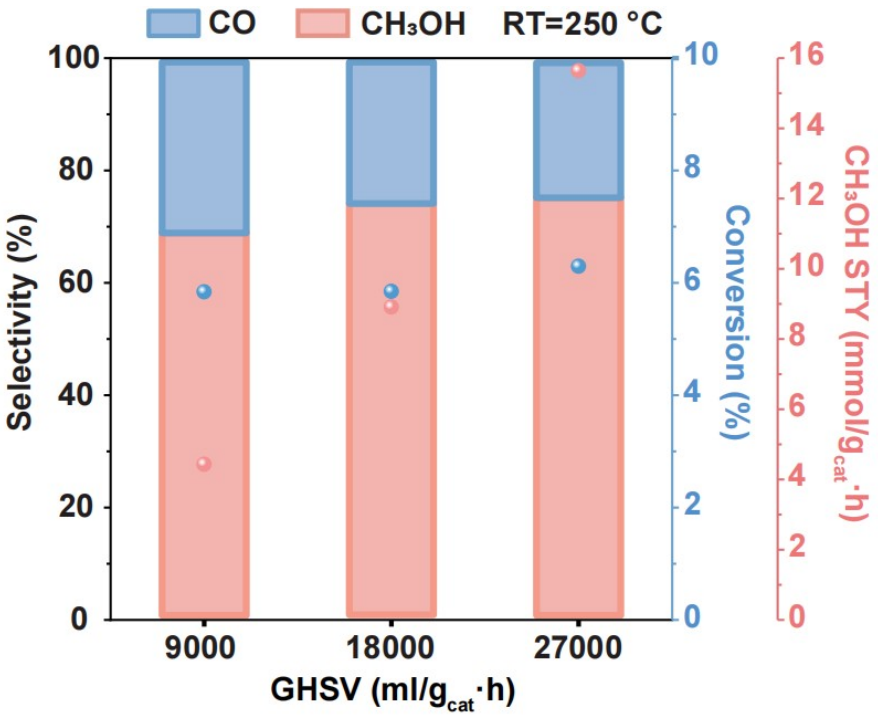

Fig. S16. Effect of GHSV on CO_2 conversion product selectivity and methanol STY over the optimized 15% Cu-ZnO/NOMC(0.2)-550 catalyst. (Reaction conditions: 250 °C, 3.0 MPa, H_2/CO_2 = 3:1).

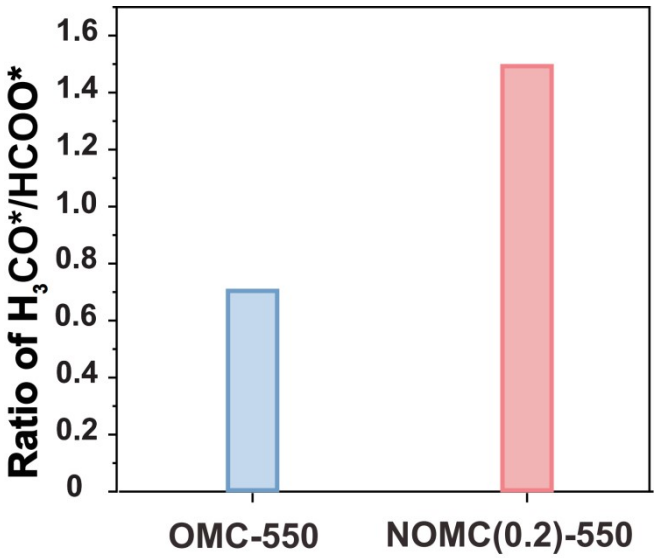

Fig. S17. Comparison of the ratio of the relative peak intensities of H_3CO^* to HCOO* species on both catalysts at a reaction temperature of 300 °C (Reaction conditions: gas flow rate = 15 ml/min, $H_2/CO_2/N_2$ = 72/24/4, P = 3.0 MPa).

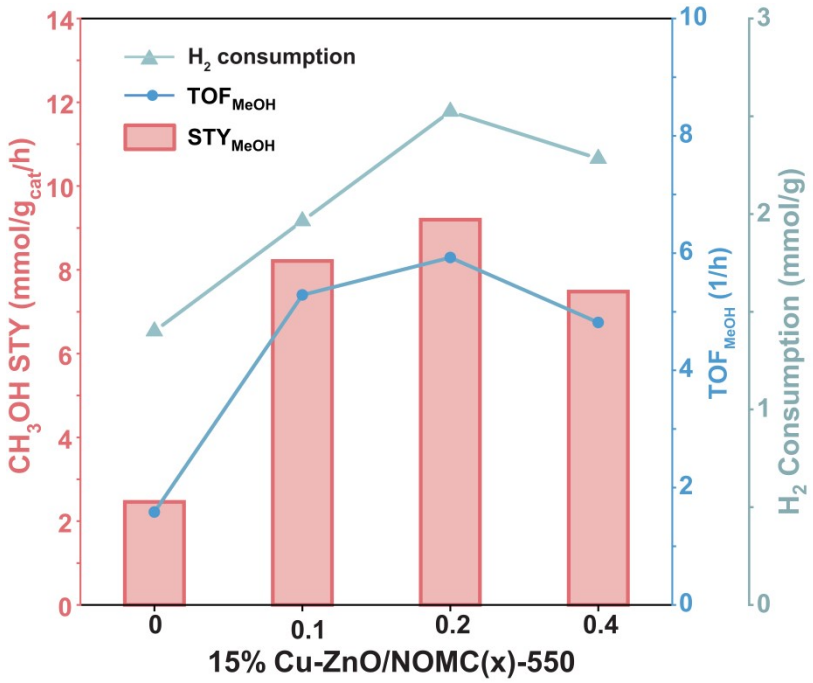

Fig. S18. Correlation between H_2 consumption (from H_2-TPR), methanol turnover frequency (TOF_{CH3OH}), and methanol space-time yield (STY_{CH3OH}) for 15% Cu-ZnO/NOMC(x)-550 catalysts with different N doping ratios (x = 0, 0.1, 0.2, 0.4). (Standard reaction conditions: Reaction Temp 250 ℃, 3.0 MPa, GHSV=18000 mL g cat^{-1} h^{-1}).

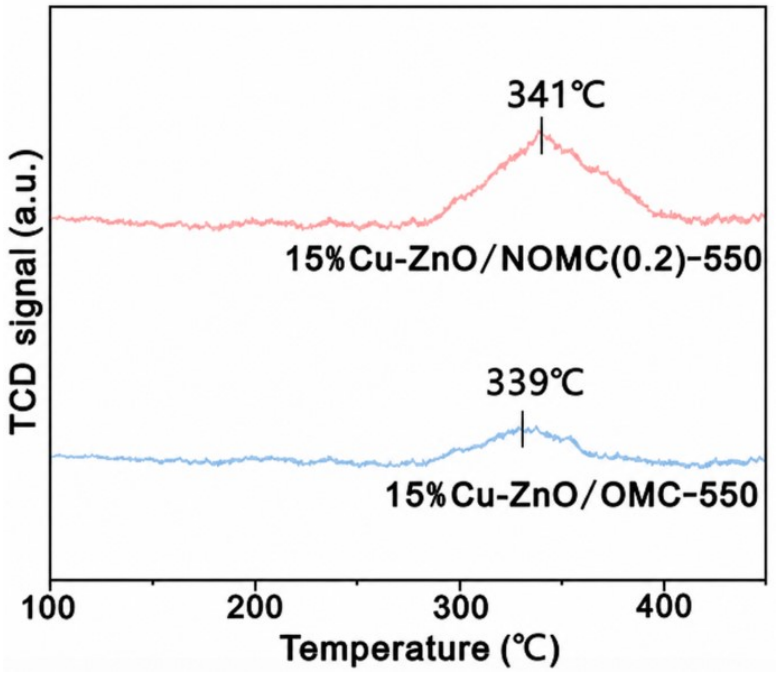

Fig. S19. H_2-TPD profiles of undoped and N-doped Cu-ZnO catalysts. The 15%Cu-ZnO/NOMC(0.2)-550 catalyst exhibits a higher H_2 desorption temperature (341 °C) and a much larger H_2 desorption peak compared to the undoped 15% Cu-ZnO/OMC-550 (339 °C), indicating a stronger H_2 adsorption ability and a larger H_2 adsorption capacity. This enhanced adsorption strength reflects the improved ability of the N-doped catalyst to activate H_2 and generate surface-active H* species, which facilitates the rate-determining step of formate hydrogenation in CO_2-to-methanol synthesis.

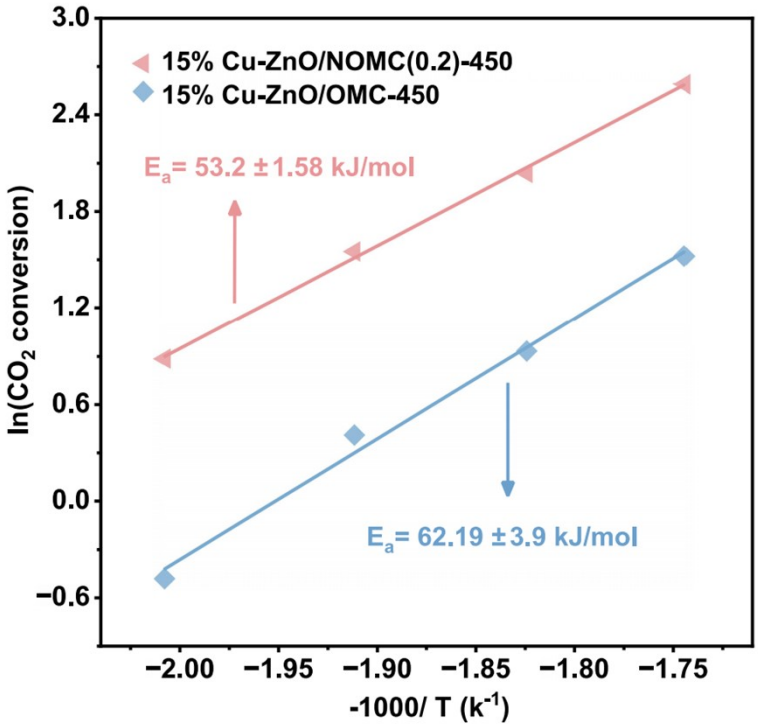

Fig. S20. Arrhenius plots for CO_2 hydrogenation over 15% Cu-ZnO/OMC-450 and 15% Cu-ZnO/NOMC-450 catalysts, with the calculated apparent activation energies (Ea) indicated.

Table S1. Types and quantities of chemicals required to prepare a series of pure and N-doped carbon support precursors with various nitrogen doping levels.

Name	**OMC**	**NOMC (0.1)**	**NOMC (0.2)**	**NOMC (0.4)**
N/C molar Ratio	0:10	1:9	2:8	4:6
DI water	162 ml	162 ml	162 ml	162 ml
3-(3-Aminomethyl) phenol	0 mmol	3 mmol	6 mmol	12 mmol
Resorcinol	30 mmol	27 mmol	24 mmol	18 mmol
Hexamethylenetetramine	7.5 mmol	7.5 mmol	7.5 mmol	7.5 mmol
Pluronic® F127	6.6 g	6.6 g	6.6 g	6.6 g

Table S2. Summary of average Cu crystalline sizes calculated using the (111) diffraction peak by Scherrer equation.

Catalyst name	Fresh Average Cu crystallites size (nm)	Spent Average Cu crystallites size (nm)
5% Cu-ZnO/ NOMC (0.1)-550	17.1	18.4
10% Cu-ZnO/ NOMC (0.1)-550	19.2	20.4
15% Cu-ZnO/ NOMC (0.1)-550	20.7	22.8
15% Cu-ZnO/ NOMC (0.2)-550	17.9	19.5
15% Cu-ZnO/ NOMC (0.4)-550	18.7	20.0
15% Cu-ZnO/ OMC-550	25.5	32.6

Table S3. Physicochemical properties of Cu-ZnO/NOMC and Cu-ZnO/OMC catalyst

Sample	D_{cu} (%)	N_{Cu} (μmol/g_{cat})	S_{cu} (m^2/g_{cat})[a]	TOF (1/h)[b]
15% Cu-ZnO/OMC-550	38.7	912.4	37.4	3.9
15% Cu-ZnO/NOMC(0.2)-550	65.8	1551.0	63.6	6.1

[a] S_{Cu} was measured by N_2O-titration, [b] TOF $_{MeOH-Cu}$ was determined by STY_{MeOH} at 250 °C divided by N_{Cu}.0

Table S4. Methanol STY of catalysts in this study compared to other Cu-based catalysts reported in the literature (only the best STY values are shown for the catalysts).

Sample	Cu %	ZnO %	P (Mpa)	T (℃)	Conv. CO_2 (%)	Sel. CH_3OH (%)	STY CH_3OH ($mmol/g_{cat}/h$)	STY CH_3OH ($mmol/g_{Cu}/h$)	Ref.
15% Cu-ZnO/NOMC(0.2)-550	**7.5**	**7.5**	**3**	**250**	**5.8**	**74.2**	**9.2**	**65.0**	**This work**
15% Cu-ZnO/OMC-550	**7.5**	**7.5**	**3**	**250**	**2.6**	**64.0**	**3.6**	**31.2**	
$Cu/ZnO/Al_2O_3$	54	17	4	300	9.1	60.2	7.5	13.9	6
CuZnAl@HT (40%)	38.1	14.8	3	250	6.16	74.7	1.3	3.4	7
CuZnAl-4	28.8	15.7	4	240	18.3	58.9	1.5	5.1	8
$Cu/Zn/Al-CO_3$	40.6	20.3	5	230	12.5	50.3	2.7	6.6	9
Cu/Zn/Al-F	41.3	21.1	5	230	12.5	59.7	3.0	7.3	
Cu-ZnO	10	90	5	250	11.7	36.1	1.0	94.6	10
CuZn@ZSM-5	2.1	1	4	260	2.0	66.6	2.9	138.1	11
Cu/ZnOx@ Na-ZSM-5	3.2	2.2	3	250	10.6	80.3	5.5	170.3	12
Cu/ZnOx/ Na-ZSM-5	3.7	2.8	3	250	6.7	74.5	3.2	86.2	
CuZn@UiO-bpy	6.9	6.0	4	250	3.3	100	0.1	1.2	13
$Cu/ZnO/Al_2O_3/ZrO_2$	48.4	22.2	3	250	25.9	61.5	6.8	14.1	14
CuZnAl	35	33.1	3	240	13.5	44	5.9	16.9	15
CuZnAlZr	46	23.3	5	270	24.5	57.6	6.9	15.0	16
Cu(ZnGa)-microwave	16.2	59	3	260	12.7	36.5	4.2	25.9	17
$Cu-ZnO-ZrO_2$-CB	45.7	22.5	3	240	16	48.7	8.3	18.2	18
CZZA/rGO	6.4	4.8	2	240	14.7	78.9	7.5	117.4	19
$Cu-ZnO-ZrO_2-SiO_2$	28.8	21.6	2	240	3	70.1	3.5	12.2	20
$Cu-ZnO-ZrO_2$-LDH	12.2	9.6	3	250	4.9	78.3	0.7	6.0	21
$Cu-ZnO-ZrO_2$	45.7	24.5	3	250	7.5	59.5	0.9	1.9	

Cu-ZnO-$SrTiO_3$	29.8	15.1	3	250	20.2	46.6	3.0	10.1	22
RE-$CuZnO/SiO_2$	15.1	11.2	3	250	11.4	35.5	3.1	20.6	23
30Cu/Zn/ms-SiO_2	22.9	9.5	3	220	14.1	57.2	1.7	7.6	24

Reference

[1] P. B. Weisz, C. D. Prater, Interpretation of measurements in experimental catalysis, *Adv. Catal.*, 1954, **6**, 143–196.

[2] L. F. Brown, Mass transfer in heterogeneous catalysis, *J. Catal.*, 1970, **18**, 240–241.

[3] N. Wakao, J. M. Smith, Diffusion in catalyst pellets, *Chem. Eng. Sci.*, 1962, **17**, 825–834.

[4] N. Epstein, On tortuosity and the tortuosity factor in flow and diffusion through porous media, *Chem. Eng. Sci*., 1989, **44**, 777–779.

[5] J. Zhong, X. Yang, Z. Wu, B. Liang, Y. Huang and T. Zhang, *Chem. Soc. Rev.*, 2020, **49**, 1385–1413.

[6] C. Meng, G. Zhao, X.-R. Shi, P. Chen, Y. Liu and Y. Lu, *Sci. Adv.*, 2021, **7**, eabi6012.

[7] X. Fang, Y. Men, F. Wu, Q. Zhao, R. Singh, P. Xiao, T. Du and P. A. Webley, *Chem. Eng. J.*, 2019, **378**, 122052.

[8] C. Zhang, H. Yang, P. Gao, H. Zhu, L. Zhong, H. Wang, W. Wei and Y. Sun, *J. CO2 Util.*, 2017, **17**, 263–272.

[9] P. Gao, F. Li, L. Zhang, N. Zhao, F. Xiao, W. Wei, L. Zhong and Y. Sun, *J. CO2 Util.*, 2013, **2**, 16–23.

[10] T. Fujitani, M. Saito, Y. Kanai, T. Watanabe, J. Nakamura and T. Uchijima, *Appl. Catal., A*, 1995, **125**, L199–L202.

[11] H. Ding, J. Zhang, W. Feng, Q. Yao, L. Zhang, Y. Ren, L. Ye, B. Yue and H. He, *Nanomaterials*, 2023, **13**, 3053.

[12] W.-G. Cui, Y.-T. Li, L. Yu, H. Zhang and T.-L. Hu, *ACS Appl. Mater. Interfaces*, 2021, **13**, 18693–18703.

[13] B. An, J. Zhang, K. Cheng, P. Ji, C. Wang and W. Lin, *J. Am. Chem. Soc.*, 2017, **139**, 3834–3840.

[14] Y. Wang, S. Kattel, W. Gao, K. Li, P. Liu, J. G. Chen and H. Wang, *Nat. Commun.*, 2019, **10**, 1166.

[15] F. Arena, G. Mezzatesta, G. Zafarana, G. Trunfio, F. Frusteri and L. Spadaro, *Catal. Today*, 2013, **210**, 39–46.

[16] X. Dong, F. Li, N. Zhao, F. Xiao, J. Wang and Y. Tan, *Appl. Catal., B*, 2016, **191**, 8–17.

[17] W. Cai, P. R. de la Piscina, J. Toyir and N. Homs, *Catal. Today*, 2015, **242**, 193–199.

[18] G. Bonura, M. Cordaro, C. Cannilla, F. Arena and F. Frusteri, *Appl. Catal., B*, 2014, **152–153**, 152–161.

[19] Y. J. Fan and S. F. Wu, *J. CO2 Util.*, 2016, **16**, 150–156.

[20] T. Phongamwong, U. Chantaprasertporn, T. Witoon, T. Numpilai, Y. Poo-arporn, W. Limphirat, W. Donphai, P. Dittanet, M. Chareonpanich and J. Limtrakul, *Chem. Eng. J.*, 2017, **316**, 692–703.

[21] X. Fang, Y. Men, F. Wu, Q. Zhao, R. Singh, P. Xiao, T. Du and P. A. Webley, *J. CO2 Util.*, 2019, **29**, 57–64.

[22] Y. Liu, X. Wang, Z. Wang, C. Chen, J. Song, L. Zhang, W. Bao, B. Sun, L. Wang and D. Liu, *ACS Catal.*, 2024, **14**, 12610–12622.

[23] K. Chen, J. Yu, B. Liu, C. Si, H. Ban, W. Cai, C. Li, Z. Li and K. Fujimoto, *J. Catal.*, 2019, **372**, 163–173.

[24] Y. Jiang, H. Yang, P. Gao, X. Li, J. Zhang, H. Liu, H. Wang, W. Wei and Y. Sun, *J. CO2 Util.*, 2018, **26**, 642–651.